Front. Phys., 2013, 8(5): 475–490
DOI 10.1007/s11467-013-0384-y

REVIEW ARTICLE

Optomechanical sensing with on-chip microcavities

Yi-Wen Hu, Yun-Feng Xiao*, Yong-Chun Liu, Qihuang Gong†

State Key Laboratory for Artificial Microstructure and Mesoscopic Physics, School of Physics, Peking University, Beijing 100871, China

*Corresponding authors. *yfxiao@pku.edu.cn, www.phy.pku.edu.cn/~yfxiao/; †qhgong@pku.edu.cn*

Received June 21, 2013; accepted August 23, 2013

The coupling between optical and mechanical degrees of freedom has been of broad interest for a long time. However, it is only until recently, with the rapid development of optical microcavity research, that we are able to manipulate and utilize this coupling process. When a high Q microcavity couples to a mechanical resonator, they can consolidate into an optomechanical system. Benefitting from the unique characteristics offered by optomechanical coupling, this hybrid system has become a promising platform for ultrasensitive sensors to detect displacement, mass, force and acceleration. In this review, we introduce the basic physical concepts of cavity optomechanics, and describe some of the most typical experimental cavity optomechanical systems for sensing applications. Finally, we discuss the noise arising from various sources and show the potentiality of optomechanical sensing towards quantum-noise-limited detection.

Keywords optical microcavities, mechanical resonators, cavity optomechanics, optical sensing, integrated photonics

PACS numbers 42.50.Lc, 42.50.Wk, 42.60.Da, 42.79.Pw, 07.10.Cm

Contents

1 Introduction

Optical forces were noticed dating back to 17th century since Johannes Kepler ascribed the deflection of the tails of comet to solar radiation [1, 2]. Today, optical forces are widely used in optical trapping [3], a technique that uses a highly focused laser beam to manipulate microscopic dielectric objects or even single atoms and ions. In the area of optical cavity, it was first studied in large scale Fabry–Pérot (FP) interferometers used for high-precision measurement, such as gravitational wave detection [4].

The canonical optomechanical system, shown in Fig. 1(a), is an FP cavity consisting of a rigid mirror and a movable mirror attached to a spring. The optical field in the cavity builds up in amplitude as it bounces back and forth between the two mirrors. The huge intracavity field exerts force on the movable mirror at each reflection, which detunes the resonant frequency of the FP cavity. As a result, the optical field is coupled to the mechanical oscillation of the movable mirror. Similar effects exist for whispering gallery mode (WGM) microcavity [5] where the large intracavity field circulating within the cavity applies optical force upon its boundary [Fig. 1(b)] and excites mechanical radial breathing modes [Fig. 1(c)].

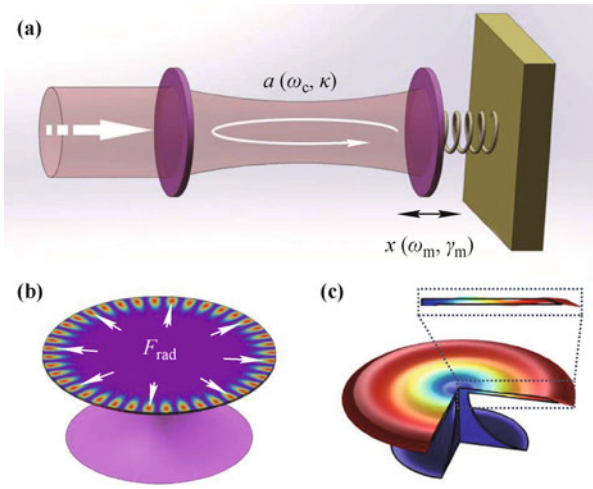

Fig. 1 **(a)** Schematics of an FP cavity with a movable end mirror. **(b)** Illustration of a microdisk cavity and the radiation forces resulting from the circulating optical power. The calculated electromagnetic field profile is mapped on the disk. **(c)** Simulated fundamental radial breathing mode of the microdisk. The inset shows the cross section view of the structure deformation. Black lines denote the initial position of the boundaries.

With improved understanding of the basic physics of optomechanical interactions and rapid progress in high quality factor (Q) microcavities and mechanical resonators, the realm of micro/nano photonics sees the possibility of integrating optomechanical devices within photonic circuits [6–8]. Conventional photonic circuits are largely immobilized because methods for reconfiguring their response are limited. Optical forces in integrated photonics reveal an exciting new approach to flexible, all-optical tuning and reconfiguration of on-chip microphotonic devices. Moreover, cavity-enhanced coupling between optical and mechanical degrees of freedom can boost the sensitivity and even allows quantum level measurement.

Over the past years, there have already been some reviews covering about cavity optomechanics, but they mainly focused on quantum phenomenon [9–13], or general applications of optical forces [6, 14]. For the past decade, highly compact and fast response optomechanical sensors have developed quickly, which may act as important elements in future ubiquitous sensor networks [15]. For the purpose of this review, we will focus on the basic principles and practical realizations of optomechanical sensing with on-chip optical microcavities.

2 Principles of optomechanical coupling

Optical microcavities confine light within small volumes and store strong optical power on their resonant frequencies [5, 16]. Compared with conventional optical cavities in the macroscale, the smaller-sized microcavities allow densely packaged optical components, and the intrinsic high quality (Q) factors of some microcavities, such as a microtoroid supporting WGMs [17], result in reduced loss in photonic circuits. In the recent decade, the basic research of their properties [18–20] is gradually and steadily extended to applied research including laser sources [21–25], modulators [26], filters [27], delay lines [28], switches [29], and biosensors [30–34].

Mechanical resonators are typically used in electronic circuits to generate signals of a precise frequency. Like their optical parallel, mechanical resonators also benefit a lot from the advances in nanotechnology. The development of nano-electro-mechanical systems (NEMS) endows them with unprecedented ability to detect physical quantities such as displacement, force, mass, charge and inertial motion [35–38]. When coupled with optical resonators, nanomechanical resonators can be used to explore the quantum properties of mechanical systems.

In this section we provide a brief description of optical microcavity, mechanical resonator and their coupling phenomena. Although quantum optomechanics is not our main focus in this review, it is still necessary to understand the fundamentals of optomechanical interaction, especially when discussing the optomechanical phenomena in the latter part of this Section and quantum noise limited sensing in Section 5. For more detailed information about the theory of cavity optomechanics, readers may refer to some textbooks [39, 40] and other reviews [12, 13].

2.1 Optical microcavity

For an optical microcavity, the equation of motion of the optical field can be written as

$$\dot{a} = \mathrm{i}\Delta a - \frac{\kappa}{2}a + \sqrt{\kappa_{\mathrm{ex}}}a_{\mathrm{in}} \tag{1}$$

Here $\kappa = \kappa_{\mathrm{in}} + \kappa_{\mathrm{ex}}$ refers to the total decay rate of the cavity mode, with κ_{in} being the intrinsic decay rate and κ_{ex} being the external coupling rate. As a classical correspondence, the optical field annihilation operator a represents the normalized amplitude of the electric field such that cavity power $P_{\mathrm{c}} = \hbar\omega_{\mathrm{L}}\langle a^{\dagger}a\rangle/\tau_{\mathrm{rt}}$, where $\tau_{\mathrm{rt}} = nL/c$ the round trip time of a photon circulating in the cavity with L the round trip length and n the cavity refractive index. a_{in} represents the input field, normalized with $P_{\mathrm{in}} = \hbar\omega_{\mathrm{L}}\langle a_{\mathrm{in}}^{\dagger}a_{\mathrm{in}}\rangle$. $\Delta = \omega_{\mathrm{L}} - \omega_{\mathrm{c}}$ is the detuning between the laser and the cavity mode. The steady-state solution of Eq. (1) reads

$$\langle a\rangle = \frac{\sqrt{\kappa_{\mathrm{ex}}}\langle a_{\mathrm{in}}\rangle}{\kappa/2 - \mathrm{i}\Delta} \tag{2}$$

To characterize the ability of cavity for power enhancement, we introduce the cavity build-up factor defined by $G = P_c/P_{in}$. For a 50 μm radius silica microtoroid cavity with $Q \sim 10^8$, G can exceed 10^5.

According to the standard input–output formalism in the microcavity [41], the field amplitude coupled back into outside is given by

$$a_{out} = a_{in} - \sqrt{\kappa_{ex}}a \tag{3}$$

Now we obtain the transmission function generally detected in experiment

$$T = \left|\frac{\langle a_{out}\rangle}{\langle a_{in}\rangle}\right|^2 = \left|\frac{(\kappa_{in}-\kappa_{ex})/2 - i\Delta}{(\kappa_{in}+\kappa_{ex})/2 - i\Delta}\right|^2 \tag{4}$$

which is a typical Lorentzian lineshape.

2.2 Mechanical resonator

The Newton equation of motion for a harmonic oscillator with effective mass m_{eff} is

$$\ddot{x} + \gamma_m\dot{x} + \omega_m^2 x = \frac{1}{m_{eff}}[F_{ex}(t) + F_L(t)] \tag{5}$$

where $F_{ex}(t)$ denotes the external force driving the mechanical mode, and $F_L(t)$ is the noise force, typically the Langevin force originating from thermal Brownian motion. Generally we concern about the mechanical displacement spectrum, which can be obtained through the Fourier transformation of Eq. (5)

$$x(\omega) = \chi_{xx}(\omega)[F_{ex}(\omega) + F_L(\omega)] \tag{6}$$

$$\chi_{xx}(\omega) \equiv \frac{1}{m_{eff}(\omega_m^2 - \omega^2) - im_{eff}\gamma_m\omega} \tag{7}$$

Here $\chi_{xx}(\omega)$ is termed as the mechanical susceptibility.

If we replace the classical mechanical quantities with phonon creation $b^\dagger$ and annihilation b operators

$$x = x_{zpf}(b + b^\dagger), \quad p = -im_{eff}\omega_m x_{zpf}(b - b^\dagger) \tag{8}$$

where $x_{zpf} = \sqrt{\hbar/(2m_{eff}\omega_m)}$ the zero point fluctuation ($x_{zpf}^2 = \langle 0|x^2|0\rangle$), then the Hamiltonian of the mechanical harmonic oscillator can be expressed as

$$H = \hbar\omega_m(b^\dagger b + 1/2) \tag{9}$$

2.3 Optomechanical coupling

Now we turn to a system composed of an optical mode (ω_c) and a mechanical mode (ω_m). If they are uncoupled, the free Hamiltonian of the system is

$$H_0 = \hbar\omega_c a^\dagger a + \hbar\omega_m b^\dagger b \tag{10}$$

Taking the FP cavity shown in Fig. 1(a) for example, when the cavity length changes x by some kind of forces (external, internal or noise force), it shifts the optical resonant frequency by $\delta\omega$

$$\omega_c(x) = \omega_c + \delta\omega \simeq \omega_c + x\frac{\partial\omega_c}{\partial x} \tag{11}$$

Thus, the optical and mechanical modes are coupled together. We can define optomechanical coupling coefficient, $g_{om} \equiv \partial\omega_c/\partial x$. This is the key parameter in optomechanics since it links optical with mechanical freedoms. This mechanical modulation of cavity resonant frequency can be easily observed through cavity transmission spectrum. The interaction Hamiltonian from optomechanical coupling should be written as

$$H_{int} = \hbar g_{om} x a^\dagger a = \hbar g_0 a^\dagger a(b + b^\dagger) \tag{12}$$

Here $g_0 \equiv g_{om}x_{zpf}$ denotes the single photon coupling strength. This implies the existence of optical force, which can be expressed as a derivative of H_{int} with respect to mechanical displacement x

$$F_{opt} = -\frac{\partial H_{int}}{\partial x} = -\hbar g_{om} a^\dagger a \tag{13}$$

In optomechanical sensing, on the one hand, this optical force can be used to construct novel tunable sensors and they show distinct advantages over other traditional tuning method on bandwidth, speed and efficiency [42]. On the other hand, the optical force introduces an additional noise source, which should be analyzed carefully when sensing toward quantum limit, which will be discussed specifically in Section 5. Considering F_{opt} and ignoring other forces in Eq. (5), we have the coupled optomechanical equation of motion in classical form

$$\dot{\alpha} = i(\Delta + g_{om}x)\alpha - \frac{\kappa}{2}\alpha + \sqrt{\kappa_{ex}}\alpha_{in} \tag{14}$$

$$\ddot{x} = -\gamma_m\dot{x} - \omega_m^2 x + \frac{\hbar g_{om}|\alpha|^2}{m_{eff}} \tag{15}$$

where α and α_{in} are the classical correspondence of a and a_{in}, respectively. Note that nonlinear differential equations Eqs. (14) and (15) are the basis of many optomechanical nonlinear phenomena.

2.4 Optomechanical phenomena

The coupling between optical and mechanical fields leads to both static and dynamical optomechanical effects. For the static case, the mechanical equilibrium position will be changed and optical bistability may occur. For the dynamical case, the finite cavity decay rate κ introduces retardation effect between the motion and the optical force, hence the so-called optomechanical dynamical backaction. In the following, we discuss the above optomechan-

ical phenomena.

2.4.1 Optical bistability

From Eq. (13), optical force $F = -\hbar g_{\rm om} n_{\rm c}(x)$. Due to optomechanical coupling, $n_{\rm c}(x)$ depends on mechanical displacement x [see Eq. (14)]

$$n_{\rm c}(x) = \alpha^*(x)\alpha(x) = \frac{n_{\rm c}^{\max}}{1 + 4(\Delta + g_{\rm om}x)^2/\kappa^2} \tag{16}$$

Therefore, the potential $V_{\rm int}$ (corresponding to $H_{\rm int}$ in system Hamiltonian) resulting from optical force can be written as

$$V_{\rm int} = -\frac{1}{2}\hbar\kappa n_{\rm c}^{\max} \arctan[2(\Delta + g_{\rm om}x)/\kappa] \tag{17}$$

However, since x is also coupled with α as shown in Eq. (15), there may exist different static solutions for the same detuning Δ. Alternatively speaking, there exist more than one equilibrium position x, leading to what we term as optical bistability (Fig. 2). This bistability phenomenon has been observed in macroscopic FP cavities [43] and also in microcavities [44, 45].

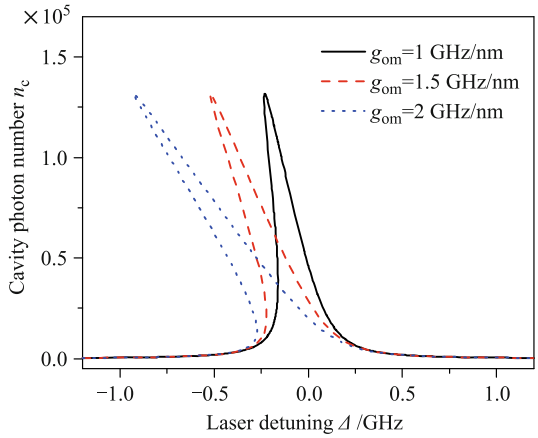

Fig. 2 Optical bistability in an optomechanical system. A hysteresis behavior can be clearly seen from the dependence of cavity photon number $n_{\rm c}$ on laser detuning Δ. The calculation parameters are set as follows: $m_{\rm eff}$=30 mg, $\omega_{\rm m}$=2000 Hz, $\kappa = 2\kappa_{\rm ex}$=1.5×10^8 Hz, $P_{\rm in}$=1 μW, $g_{\rm om}$ is given in the figure.

2.4.2 Optical spring and damping effect

To analyze the dynamical behavior, we make a linear approximation ($\alpha = \bar{\alpha} + \delta\alpha$) to Eqs. (14) and (15). Expressing them in the frequency domain, we obtain

$$-{\rm i}\omega\delta\alpha = ({\rm i}\Delta - \frac{\kappa}{2})\delta\alpha + {\rm i}g_{\rm om}\bar{\alpha}x \tag{18}$$

$$-m_{\rm eff}\omega^2 x = -m_{\rm eff}\omega_{\rm m}^2 x + {\rm i}\omega m\gamma_{\rm m}x + \hbar g_{\rm om}(\bar{\alpha}^*\delta\alpha + \bar{\alpha}\delta\alpha^*) \tag{19}$$

Compared to the uncoupled case, the optomechanical influence can be considered as the change of mechanical susceptibility from $\chi_{\rm xx}(\omega)$ to $\tilde{\chi}_{\rm xx}(\omega)$,

$$\frac{1}{\tilde{\chi}_{\rm xx}(\omega)} - \frac{1}{\chi_{\rm xx}(\omega)} = \hbar g_{\rm om}^2|\bar{\alpha}|^2\left[\frac{1}{(\Delta+\omega) + {\rm i}\kappa/2} + \frac{1}{(\Delta-\omega) - {\rm i}\kappa/2}\right] \tag{20}$$

Combined with Eq. (7), it can be found that the eigenfrequency and damping rate of mechanical mode have been modified due to optomechanical coupling. The physical origin of such phenomena comes from the nonlinear and non-adiabatic dynamics associated with the mechanical displacement and the internal cavity power. Quantitatively, since $1/\chi_{\rm xx} = m_{\rm eff}(\omega_{\rm m}^2 - \omega^2) - {\rm i}m_{\rm eff}\gamma_{\rm m}\omega$, the real part of Eq. (20) should correspond to the mechanical eigenfrequency change (see Fig. 3, left panel)

$$\delta\omega_{\rm m}(\omega) = \frac{g_0^2|\bar{\alpha}|^2\omega_{\rm m}}{\omega}\left[\frac{\Delta+\omega}{(\Delta+\omega)^2 + \frac{\kappa^2}{4}} + \frac{\Delta-\omega}{(\Delta-\omega)^2 + \frac{\kappa^2}{4}}\right] \tag{21}$$

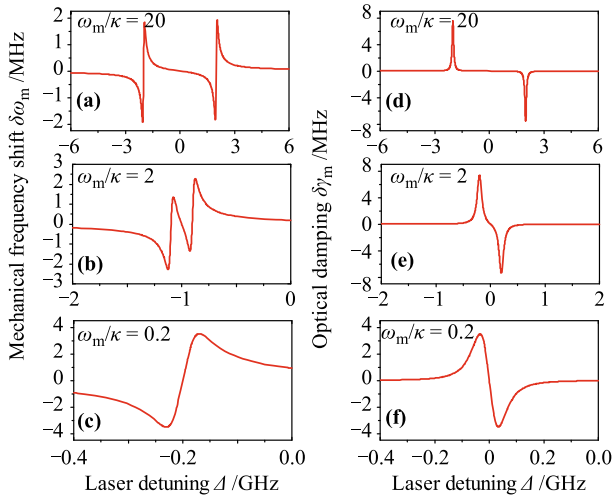

Fig. 3 Optical spring and optical damping effects calculated from Eq. (21) and (22) with different $\omega_{\rm m}/\kappa$. **(a–c)** Optical spring effect. **(d–f)** Optical damping effect. Parameters are set as follows: $m_{\rm eff}$ = 10 pg, κ = 100 MHz, $g_{\rm om}$ = 0.03 GHz/nm, $P_{\rm in}$ = 1 μW.

This frequency shift can also be regarded as modification of structure stiffness since $\omega_{\rm m} = \sqrt{k/m_{\rm eff}}$ (k is the stiffness coefficient) and is just the so-called "optical spring effect". In experiment, the mechanical stiffness of a nanobeam has been increased by 200 times [46].

As mentioned above, the imaginary part of Eq. (20) should be the optical damping term (see Fig. 3, right panel)

$$\gamma_{\rm opt} = \delta\gamma_{\rm m} = \frac{g_0^2|\bar{\alpha}|^2\omega_{\rm m}}{\omega}\left[\frac{\kappa}{(\Delta+\omega)^2 + \frac{\kappa^2}{4}} - \frac{\kappa}{(\Delta-\omega)^2 + \frac{\kappa^2}{4}}\right] \tag{22}$$

This effect is the basis for intrinsic optomechanical cooling [47–49]. When $\omega_m \ll \kappa$, as shown in Figs. 4(c) and (f) the mechanical oscillator will be spring softened for a red-detuned laser beam ($\Delta < 0$), and spring-hardened for a blue-detuned laser ($\Delta > 0$). However when in the resolved sideband regime ($\omega_m > \kappa$), the optical spring effect vanishes at certain detunings [Figs. 4(a) and (b)] and the radiation pressure contributes only to cooling or amplification [Figs. 4(d) and (e)].

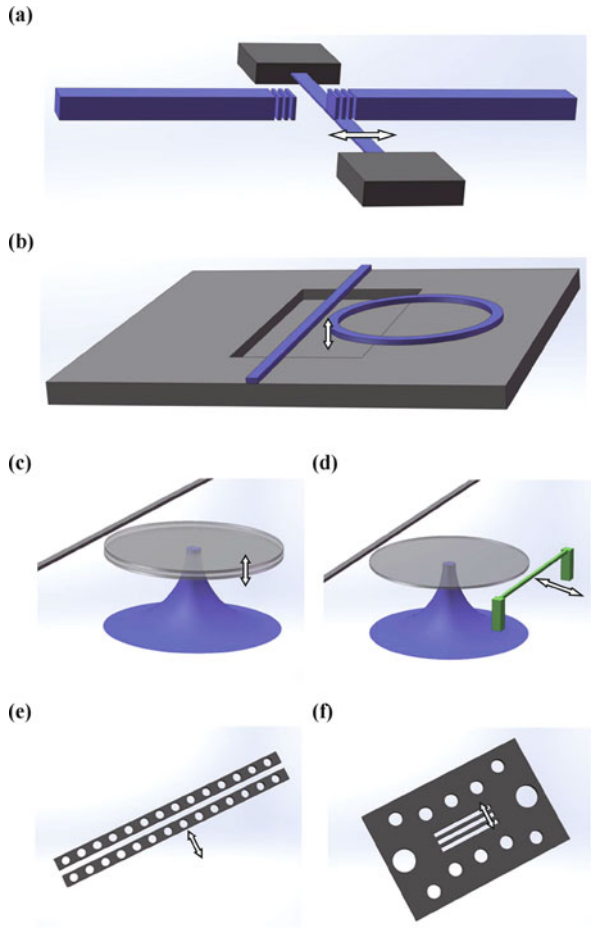

Fig. 4 Schematics of some representative on-chip optomechanical configurations. **(a)** FP cavity with one of the Bragg mirrors embedded in a mechanical beam. **(b)** Released microring cavity coupled with substrate. **(c)** Double-disk cavity. **(d)** Microdisk coupled with a mechanical beam. **(e)** Photonic crystal zipper cavity. **(f)** Mechanical beams embedded in a photonic crystal cavity. The arrows denote the direction of mechanical oscillation.

In optomechanical sensing, these two phenomena provide a promising method to actively tune the mechanical Q. Specifically, when $\gamma_{opt} > 0$, they lead to mechanical cooling and the mechanical linewidth broadening; while if $\gamma_{opt} < 0$, this optomechanical coupling implies mechanical amplification and the mechanical linewidth becomes narrower, which may be employed to improve the sensitivity of some sensing applications.

3 Experimental optomechanical systems

Following pioneering microcavity optomechanics study in microtoroid systems [50, 51], a variety of alternate microphotonic device geometries have been investigated. Various mechanisms have been studied for enhancing the optical force. Below, we review some of the most typical architectures.

FP cavities are among the most widely used cavities because of their simplicity and high finesse. In on-chip optomechanical systems, there are generally two obstacles to overcome when using an FP cavity: one is to make two mirrors integrated on a chip and the other is to involve in a moving part within. A typical solution is to employ DBRs (distributed Bragg reflectors) based FP cavity [52, 53]. One DBR is fixed and the other acts as the mechanical flexible part, as shown in Fig. 4(a). However, as the DBR mirrors cannot show very high reflectivity, this resulting relatively low optical Q may limit the sensitivity of this kind of device in some applications.

Microring resonators attract a lot of attention in integrated photonic circuits due to their simple fabrication and applications in various optical communication and interconnect systems [54, 55]. Optomechanical system can be easily formed with them when a nanomechanical beam is released from a part of the microring cavity, as seen in Fig. 4(b). To overcome the damage for optical and mechanical properties while undercutting the device, Pernice *et al.* [56] added two photonic crystal couplers to support the mechanical beam. Li *et al.* [57] combined slot waveguide structure with a racetrack cavity (an extension of microring) and also obtained improved optical Q. These optimizations are important because a higher optical Q cannot only enhance the optical force, but also improve the detection sensitivity. To reduce the mechanical stiffness and increase the sensitivity of optical forces, structures of spokes and coupled rings [46] can be introduced.

WGM resonators confine optical field inside a circular dielectric by total internal reflection [58, 59]. One distinct advantage for WGM cavities over other microstructures is their ultrahigh optical Q (exceeding 10^8) due to reflow process [17]. Like other structures, many efforts have been made to decouple the optical and mechanical freedoms for WGM cavity, which is desirable for optomechanical devices because the optical and mechanical freedoms can thus separately optimized for specific applications. Generally there are two ways to undertake this problem: one is to modify the structure of the cavity itself, such as spoke-supported [60] or double-layer structures [Fig. 4(c)] [61–65]; the other is to introduce

mechanical resonators from outside, such as membranes, cantilevers or beams [Fig. 4(d)] [66–70]. In both types of structure, there exist technological challenges to achieve high optomechanical coupling g_{om} while maintaining excellent and flexible optical and mechanical properties.

Photonic crystal microcavities can also confine light in ultra-small mode volumes and exhibit high optical Q. Much work exploits these attributes to achieve strong optomechanical effects. Chan *et al.* [71] and Eichenfield *et al.* [72] have designed and experimentally demonstrated a periodically patterned "zipper" system with large optomechanical coupling. The zipper is made up of two parallel, patterned nanobeams [as shown in Fig. 4(e)] each of which is designed to support an optical microcavity mode. Coupling between the modes gives rise to attractive and repulsive forces. In Ref. [73], a single nanobeam structure is designed and realized to confine both the optical modes and the mechanical vibration modes to the scale of the optical wavelength. Localized mechanical modes are created using a phononic band gap microcavity, analogous to the optical case. The authors suggest that the strong optomechanical coupling between optical modes (200 THz optical resonance frequency) and high-frequency mechanical modes (2 GHz mechanical resonance frequency) will allow extremely sensitive mass detection via optical readout. Notomi *et al.* theoretically analyzed microcavities in parallel photonic-crystal slabs [74]. Intriguingly, the authors suggest that if the mechanical displacement between the structures occurs faster than the response time of the optical cavity (proportional to the optical period times the optical Q), wavelength conversion will occur. This phenomenon is analogous to the frequency shifts predicted and measured in microphotonic systems with time-varying linear refractive index. Sun *et al.* [75] demonstrated a new optomechanical device system which allows highly efficient transduction of femtogram nanobeam resonators. A double-beam nanomechanical resonator is embedded in a photonic crystal slab cavity [see Fig. 4(f)]. As mechanical and optical modes are formed almost in the same area, strong optomechanical interaction exists.

In the previous discussion, we have listed out most typical cavity structures used in optomechanical sensing. In Table 1, we sum up some characteristic parameters of representative works in the past few years and several conclusions can be made from this table. First, most devices employ silicon-based material, and this results from their fabrication compatibility and excellent optical/mechanical properties. Second, vacuum condition is required to achieve high mechanical quality factor. Although the above two points are the current trends now, there are some obvious drawbacks. For example, till now the highest optical and mechanical quality factors cannot be achieved within a single material, and vacuum environment imposes relatively rigorous condition on experimental apparatus. The comparison of merits and demerits between different devices is not provided here, but it should be noted that since the optomechanical effects that can be exploited in each type of sensors are different, as is discussed in the next section, a variety of device designs are promising to find their niche in on-chip applications. Actually, optomechanics are merging with more and more optical/photonic areas. Other platforms such as optofluidics [76] and metamaterials [77] are also found to be good candidates for on chip optomechanical coupling or optical force enhancement.

4 Optomechanical sensing applications

4.1 Displacement, force and mass sensing

High-sensitive displacement sensing is the basis of many other sensing applications because the variations of many

Table 1 Summary of selected experiments on optomechanical coupling in integrated photonic devices.

Device type	Device material (opt+mech)[a]	Vacuum (Y/N)	m_{eff} /g	ω_{m} /Hz	Q_{m}[b]	Q_o[b]	g_{om} /(GHz·nm^{-1})	Year
Microtoroid-nanostring [67]	Silica+SiN[c]	Y	4.9×10^{-12}	6.74×10^{7}	4×10^{4}	4×10^{6}	0.024	2009
Double disk [61]	Silica+Silica	Y	1.45×10^{-10}	5.34×10^{7}	4070	1×10^{6}	207	2009
Double ring [46]	SiN+SiN	N	8.5×10^{-11}	1.2×10^{8}	2	6.8×10^{4}	80	2009
Slot ring-released waveguide [57]	Si+Si[c]	Y	Not given	7.4×10^{8}	2400	6×10^{4}	280[d]	2010
Waveguide-DBR cavity [53]	Si+Si	Y	6.8×10^{-9}	6.3×10^{5}	2×10^{4}	5000	28	2011
Microdisk-bend cantilever [78]	Si+Si	N	7.3×10^{-13}	14	5	1×10^{5}	3.14–19	2011
Photonic crystal zipper [79]	SiN+SiN	Y	1×10^{-8}	1.73×10^{5}	1.4×10^{6}	9500	35	2012
Microdisk-nanobeam [69]	Silica+SiN	Y	9×10^{-12}	1.8×10^{7}	4.8×10^{5}	6.5×10^{4}	0.003	2012
Photonic crystal-embedded beams [75]	Si+Si	Y	2.5×10^{-14}	6.28×10^{9}	1230	2×10^{4}	70	2012

[a] optical cavity material+mechanical resonator material.
[b] Q_{m}: mechanical Q; Q_o: optical Q.
[c] SiN: silicon nitride; Si: silicon.
[d] The value is estimated from the data provided within the reference.

other physical parameters can convert to position shift of a certain component. Generally, the mechanical displacement can be converted into optical transmission signal through optomechanical coupling coefficient $g_{\rm om}$, and read out by a photodetector or optical spectrum analyzer. Early study [Fig. 5(a)] showed that coupled microspheres have comparable or better displacement sensitivity than traditional sensors based on large-scale FP resonators [80, 81]. This sensitivity originates from the separation-induced normal modes splitting of the coupled resonators. A further improvement in sensitivity over the edge-coupled configuration was predicted for vertically coupled hemispherical resonators [81]. Although the experimental realization of such hemispheres has remained unattainable, other practical optomechanical configuration such as the double disk cavity [Fig. 5(b)] or zipper cavity, can be well employed for displacement sensing.

Displacement is linked with force by mechanical susceptibility $\chi_{\rm xx}$ as defined in Eq. (7). Force sensing is fundamental in biosensing to diagnose the dynamic process of bio-molecules [82]. In the present, force sensors based on micro-beams are widely studied [83]. Miniature Structures with high mechanical frequency and low stiffness are highly preferred here because they are more immune to environmental vibration and more sensitive. When combining with optical cavities (see Fig. 6), these sensors can enhance the ability to resolve the motion of micro-beams through $g_{\rm om}$ and improve bandwidth which is proportional to cavity optical Q [78, 84]. What's more, by applying active optical feedback (optical spring and damping effect), the mechanical properties can be modified to suppress noise [69, 85]. Another interesting application of optomechanics force sensing is the capability to compensate for or measure Casimir force [96], which has already attracted attention in MEMS technology for years [87, 88].

Mass sensors are a very important components in nanotechnological measurement. Traditionally, mass spectrometer is used for nanoparticle sensing (even single atoms). But the particle has to be ionized before the mass can be extracted. In recent years, nanomechanical

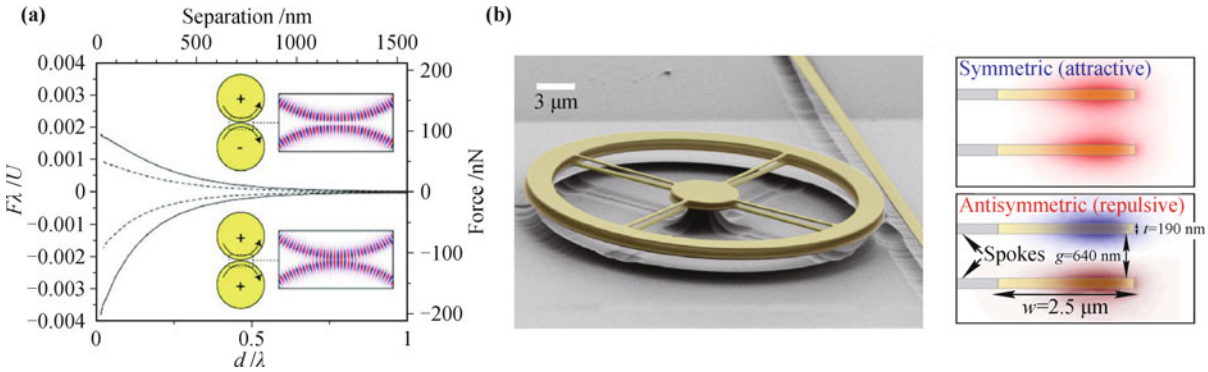

Fig. 5 Force and displacement sensing with optomechanical systems. **(a)** Optical attractive and repulsive force as a function of separation for two coupled microspheres. Asymmetric and symmetric modes are shown in the top and bottom insets. **(b)** *Left*: Scanning electron micrograph (SEM) of two double-ring microcavities. *Right*: Cross section simulation of the supported optical symmetric and asymmetric modes. The separation change of these type of structures can be rapidly detected by highly sensitive optical readout and they can both be used for force or displacement sensing. Figures reproduced with permission from (a) Ref. [80] © 2005 Optical Society of America; (b) Ref. [46] © 2009 Nature Publishing Group.

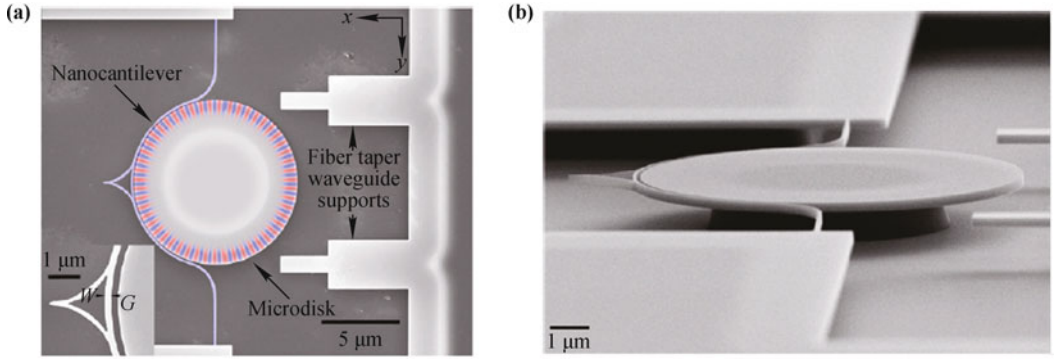

Fig. 6 **(a)** Top view SEM of a bend cantilever coupled microdisk. The nano-size sharp tip in the middle of the cantilever can be used as a probe for atomic force microscope (AFM). **(b)** Oblique view of the same structure of the cantilever-microdisk system. Reproduced from Ref. [78], Copyright © 2011 American Chemical Society.

oscillators are adopted in mass detection. They have already enabled extraordinary sensitive measurement of mass down to 1×10^{-21}g in vacuum and 1×10^{-15}g in liquid environment. Generally, the external samples with mass Δm depositing onto the surface of a mechanical resonator will lead to the resonant frequency-shift $\Delta\omega_{\rm m}$,

$$\Delta m = \frac{2m_{\rm eff}}{\omega_{\rm m}}\Delta\omega_{\rm m} \tag{23}$$

It can be clearly seen that, to achieve high mass sensitivity, resonator mass has to be low, and the mechanical frequency as well as quality factor should be high to reduce the minimum detectable frequency change. Some efforts [89, 90] using cavity optomechanics for mass sensing have been made and one distinct advantage over previous methods based on nanomechanical resonators is the all optical actuation and detection. However, the thermal and optical noise resulting from the instability of taper coupling limits the detection resolution to picograms [90]. This is because tapered waveguide coupling requires careful alignment and the slim coupling region are relatively sensitive to mechanical or other variations in the surrounding environment. To reduce this noise, free space [91–93] or integrated bus waveguide [94, 95] coupling may be an efficient scheme.

4.2 Inertial sensing

Inertial sensors are used to detect and measure acceleration, tilt, vibration, gyration. Today they are not only used in aircraft and spacecraft to form the inertial guidance system, but are also gradually entering people's everyday life. Accelerators, for example, have already become an indispensable component in many consumer electronics such as smartphones and tablet PC. Early in 2001, Lain *et al.* [96] proposed an acceleration sensor using a fiber stem supported high Q microsphere to achieve 1 mg sensitivity and 250 Hz bandwidth [Fig. 7(a)]. The relative low sensitivity resulted from the small $g_{\rm om}$ of microsphere-waveguide coupling. Actually, we can write a similar susceptibility for acceleration as in Eq. (7):

$$\chi_{\rm aa}(\omega) \equiv \frac{1}{(\omega_{\rm m}^2 - \omega^2) - {\rm i}\gamma_{\rm m}\omega} \tag{24}$$

If $\omega \ll \omega_{\rm m}$, $\chi_{\rm aa}(\omega) \sim 1/\omega_{\rm m}^2$ and we get $a(\omega) \sim x(\omega)\omega_{\rm m}^2$. On the one hand, just as mentioned in the last subsection, acceleration sensing is also based on displacement sensing, and prefers low mechanical frequency for high detection sensitivity. On the other hand, its sensitivity should also be proportional to $g_{\rm om}$ because this coefficient transduces the mechanical change to optical signal. As a result, many efforts have been done to improve these two aspects. FP cavities are still among the most extensively studied structures for optical acceleration sensing [52, 97, 98]. Although down to ng sensitivity has been achieved, to realize compact and sensitive structure is still a challenge for researchers. Zandi *et al.* [52] demonstrated an on-chip planar accelerometer. Two proof masses are connected to a DBR-based FP cavity to provide both low mechanical frequency and high efficient optomechanical transduction. This structure can achieve $g_{\rm om} \sim 40$ GHz/nm. However, the DBR structures limit optical Q to about 660, and the readout method based on traditional optical spectrum analyzer also decrease the resolution to about 400 μg. To enhance the performance, Krause *et al.* [79] make use of zipper cavity which owns similar $g_{\rm om}$ but much higher optical $Q \sim 10000$ and smaller proof mass [see Fig. 7(c)]. By measuring the transmission output from a photodetector on a lock-in amplifier, much better resolution (10 μg) can be achieved. If precise nano-size gap can be controlled, double disk structure [99] may show even better sensing performance since $g_{\rm om}$ can be as large as 1000 GHz/nm and the WGM-based cavity is also potential to own higher optical Q [61].

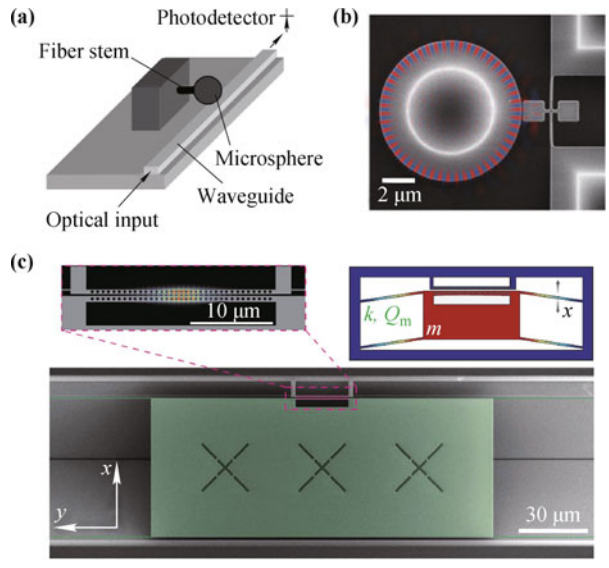

Fig. 7 Inertial sensing with optomechanical systems. **(a)** A microsphere based accelerometer. The induced flexure-arm displacement can be monitored through transmission spectrum. **(b)** A torque sensor made up of a torsional nanoscale resonator evanescently coupled to optical microdisk whispering gallery mode resonators. **(c)** SEM image of a optomechanical accelerometer base on a photonic crystal zipper cavity. *Top left*: electric field profile for the zipper cavity. The top beam is mechanically bonded on the substrate and the bottom beam is attached to the proof mass. *Top right*: Schematic displacement profile of the fundamental in-plane mechanical mode used for acceleration sensing. Figures reproduced with permission from (a) Ref. [96] © 2001 Elsevier; (b) Ref. [100] © 2013 American Institute of Physics; (c) Ref. [79] © 2012 Nature Publishing Group.

Other inertial sensors also gradually attract researchers' attention. For example, if the mechanical resonator is rotatable, a torque sensor can be formed [see Fig. 7(b)], which are valuable for ultra-sensitive optical magnetometer [101, 102].

4.3 Micro- and nanoparticle manipulation

To drag a micro/nano particle into the sensing area is one of the most important steps for particle sensing [106–108]. This area belongs to optical trapping, a quite hot research field since the end of last century, and here we will only discuss briefly a small portion of it regarding optical trapping with on-chip microcavities. Traditional trapping method are generally based on a tight focused laser beam, while major limitations of this technique are its bulky volumes and inefficient energy utilization. On chip devices, however, are highly desirable to overcome these shortcomings. In the recent years, optical waveguide based micro/nano-particle trapping and manipulation drew a lot attention due to its unique transporting feature [109]. Compared to a waveguide trapping configuration, microcavity trapping presents two primary advantages [103–105, 110]: i) the build-up factor G leads to strong optical force enhancement, and ii) cavity perturbation induced by the trapped object could serve as a highly sensitive probe for analyzing the physical properties (size, refractive index, absorption) of the objects.

To calculate the optical force exerted on the particle, an alternative way of Eq. (13) is using Maxwell stress tensor formalism [111]. The time averaged force exerted on a particle with volume V is entirely determined by the electromagnetic field on the surface ∂V:

$$\langle \boldsymbol{F} \rangle = \oint_{\partial V} \langle \overleftrightarrow{\boldsymbol{T}}(\boldsymbol{r},t) \rangle \cdot \boldsymbol{n}(\boldsymbol{r}) \mathrm{d}s \tag{25}$$

where $\overleftrightarrow{\boldsymbol{T}}(\boldsymbol{r},t)$ is the Maxwell stress tensor, and is given by $T_{\mathrm{ij}} = \epsilon(E_{\mathrm{i}}E_{\mathrm{j}} - \delta_{\mathrm{ij}}\boldsymbol{E}^2/2) + (B_{\mathrm{i}}B_{\mathrm{j}} - \delta_{\mathrm{ij}}\boldsymbol{B}^2/2)/\mu$. This expression is just an alternative way to describe the Lorentz force: $\boldsymbol{f} = \rho\boldsymbol{E} + \boldsymbol{J} \times \boldsymbol{B}$ [112], and can be divided into two parts (gradient and scattering force). When regarding a spherical non-absorbent Rayleigh particle (size much smaller than the wavelength of light), we have [113, 114]

$$\boldsymbol{F}_{\mathrm{grad}} = -\frac{n_{\mathrm{b}}^3 r^3}{2}\left(\frac{m^2-1}{m^2+2}\right)\nabla \boldsymbol{E}^2 \tag{26}$$

$$\boldsymbol{F}_{\mathrm{scat}} = \frac{\boldsymbol{I}_0}{c}\frac{128\pi^5 r^6}{3\lambda^4}\left(\frac{m^2-1}{m^2+2}\right)^2 \tag{27}$$

where $m = n_{\mathrm{p}}/n_{\mathrm{b}}$, with n_{b} and n_{p} representing the refractive index of the surrounding medium and the nanoparticle whose radius is denoted by r. As we can see, F_{grad} is proportional to r^3 while F_{scat} is proportional to r^6. This implies compared with the scattering force, the gradient forces gain rapidly in significance as the particle size decreases. Some representative works on particle manipulation employing optical microcavities are demonstrated in Fig. 8, and show good stability and accuracy. The sizes of particles used among these works, however, are still large ($\sim$ 1 μm) compared with nano-size molecules, and their optical forces are only about 1 order of magnitude larger than the forces in waveguide structures. In the recent few years, there have been some efforts concentrating on force enhancement employing higher Q microcavities or hybrid plasmonic structures [106–108, 115–118], which are inspiring for realizing high efficient manipulation (transporting, storage and routing) of nanoparticles using microcavity based platform.

5 Noise analysis and sensing towards quantum limit

In any practical measurement, signals are mixed with noises arising from contributions of various sources. Due to strong photon–phonon interaction, optomechanical devices discussed in this review can be highly susceptible to optomechanical backaction effect. This effect will modify the frequency and damping rate with as shown in Eqs. (21) and (22). As the quantity of modification is proportional to cavity power, stable optical input power and coupling should be the optimization considered first in high-sensitivity measurement. Besides, the optical power perturbation coming from the thermal-optic coefficient ($\mathrm{d}n/\mathrm{d}T$) sometimes may also have a large backaction effect.

If the input optical power is low or well stabilized, the influence of both the optomechanical and thermal-optical backaction effect can be ignored or eliminated by an offset calibration. However, there are some other noises that will always exist and can degrade sensing performance. In the following we will discuss three types of them, which are the most common physical limitations especially when taking optical sensing to the limit. The discussion is for displacement measurement and can be easily extended to other quantities.

5.1 Thermal noise

Thermal noise is one of the fundamental limits to the precision of mechanical measurement. It can be regarded as a driving force that excites the mechanical resonance with an energy around $k_{\mathrm{B}}T$. Before the discussion on thermal noise, we should first take a look at power

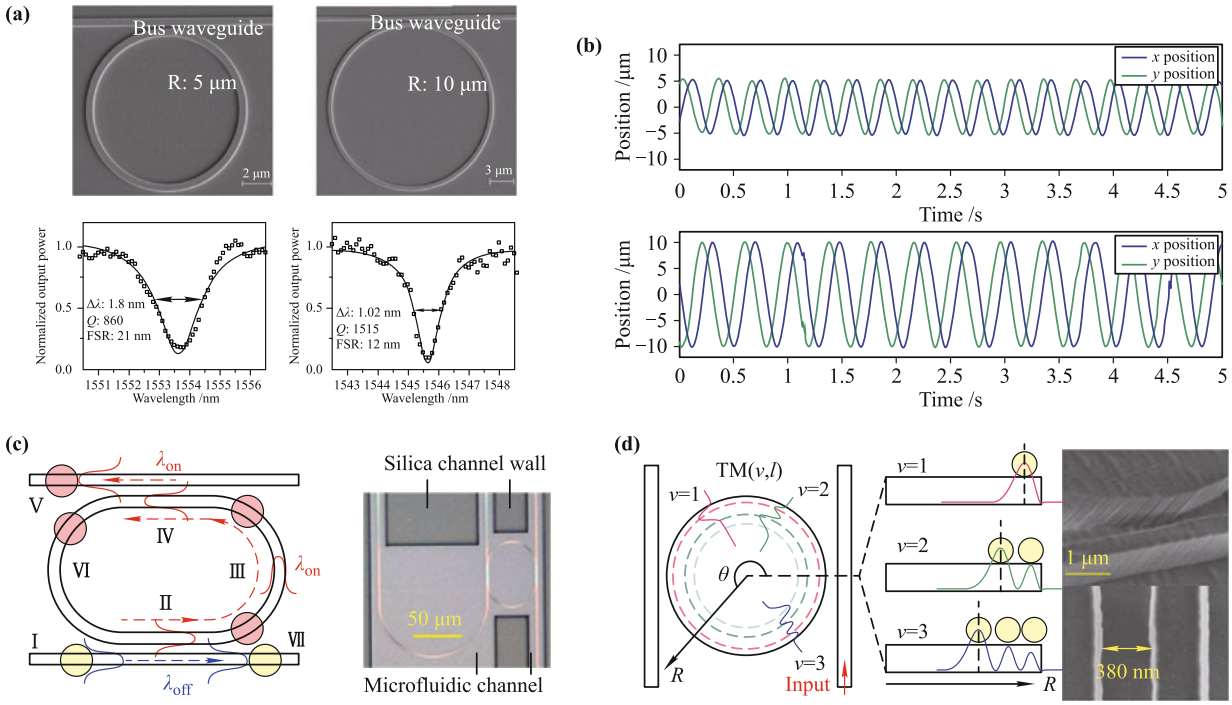

Fig. 8 Particle manipulation with optomechanical systems. **(a)** SEM images and transmission spectra of microring resonators used for optical manipulation. **(b)** Tracked positions of a single particle trapped on the 5 μm (top) and 10 μm (down) radius microring, showing a clear circular motion. **(c)** Microparticles add-drop device based on a microring resonator. **(d)** Controlled trapping of particles by exciting different order whispering gallery modes. Figures reproduced with permission from (a, b) Ref. [103] © 2010 American Chemical Society; (c) Ref. [104] © 2010 Optical Society of America; (d) Ref. [105] © 2011 Optical Society of America.

spectrum density (PSD), which is defined as the Fourier transformation of autocorrelation function. For the PSD of displacement, it is defined as

$$S_{\rm xx}(\omega) \equiv \int_{-\infty}^{+\infty} \langle x(t)x(0)\rangle {\rm e}^{{\rm i}\omega t}{\rm d}t \tag{28}$$

$S_{\rm xx}$ cannot be directly measured in practical experiment, what we measure is a average value in a limited duration.

$$\tilde{x}(\omega) = \frac{1}{\sqrt{\tau}} \int_0^{\tau} x(t){\rm e}^{{\rm i}\omega t}{\rm d}t \tag{29}$$

Wiener–Khinchin theorem tells as $\tilde{x}$ is an excellent approximation of PSD once the average time is much longer than the system's characteristic cycle

$$\lim_{\tau\to\infty} \langle |\tilde{x}(\omega)|^2\rangle = S_{\rm xx}(\omega) \tag{30}$$

And the integration of PSD gives the average of displacement

$$\int_{-\infty}^{+\infty} S_{\rm xx}(\omega)\frac{{\rm d}\omega}{2\pi} = \langle x^2\rangle \tag{31}$$

Fluctuation dissipation theorem (FDT), on the other hand, quantifies the relation between the fluctuations at thermal equilibrium and the linear response of the system. Specifically, here it links $S_{\rm xx}(\omega)$ with $\chi_{\rm xx}$ in Eq. (7)

$$S_{\rm xx}(\omega) = \frac{2\hbar}{1-{\rm e}^{\hbar\omega/(k_{\rm B}T)}}{\rm Im}\chi_{\rm xx}(\omega) \tag{32}$$

then

$$S_{\rm xx}(\omega) = \frac{2k_{\rm B}T\gamma_{\rm m}}{m_{\rm eff}} \times \frac{1}{(\omega^2-\omega_{\rm m}^2)^2+\gamma_{\rm m}^2\omega^2} \tag{33}$$

This is the spectral density of thermal motion of any simple harmonic oscillator. In many experiments, it is the thermal noise far from the resonant frequency that matters. So it is clear that, in order to keep thermal noise as low as possible, less mechanical damping and larger effective mass are preferred. From Eq. (33), the mean value of thermal motion is

$$\langle x^2\rangle_{\rm th} = \frac{k_{\rm B}T}{m_{\rm eff}\omega_{\rm m}^2} \tag{34}$$

5.2 Shot noise

The Heisenberg uncertainty relation of number-phase for coherent states determines the limited precision of $\Delta\phi = 1/(2\Delta N)$. The quantization of electromagnetic field brings fluctuation of photon number, which is described by optical shot noise. For a coherent photon state, the photon number obeys Poisson distribution:

$\Delta N = \sqrt{\bar{N}}$, where $\bar{N}$ is the mean number of photons. However, for photons circulating in a microcavity, this fluctuation is also influenced by the cavity loss and laser detuning. In Eq. (1), we have neglected the noise term $\sqrt{\kappa} f_{\rm in}$. If added and after linearization ($a = \bar{\alpha} + \delta a$), the equation of motion becomes

$$\delta\dot{a} = (\mathrm{i}\Delta - \frac{\kappa}{2}) \times \delta a + \kappa f_{\rm in} \tag{35}$$

The noise operator $f_{\rm in}$ is characterized by its averages and correlation functions. The mean value is zero: $\langle f_{\rm in}\rangle = 0$, and the non-zero correlation is

$$\langle f_{\rm in}(t)\rangle f_{\rm in}^{\dagger}(t') = \delta(t - t') \tag{36}$$

Then the photon number fluctuation can be yielded via autocorrelation function [119],

$$\begin{aligned}\Delta N^2 &= \langle a^{\dagger}(t)a(t)a^{\dagger}(0)a(0)\rangle - \langle a^{\dagger}(t)a(t)\rangle^2 \\ &= \bar{\alpha}^2\langle a(t)a^{\dagger}(0)\rangle \\ &= \bar{n}_{\rm c} \times \mathrm{e}^{\mathrm{i}\Delta t - \frac{\kappa}{2}|t|}\end{aligned} \tag{37}$$

This implies that the fluctuation of photon number should be replaced by

$$S_{\rm NN}(\omega) = \sqrt{\bar{n}_{\rm c}\frac{\kappa}{(\kappa/2)^2 + (\omega + \Delta)^2}} \tag{38}$$

On the other hand, the dependence of the phase of the output filed on mechanical displacement Δx [11]:

$$\Delta\phi = \frac{4g_{\rm om}\Delta x}{\kappa} \tag{39}$$

Then we get the displacement sensitivity ($\Delta = 0$) to

$$S_{\rm xx}^{\rm shot}(\omega) = \frac{\kappa}{16\bar{n}_{\rm c}g_{\rm om}^2}[1 + 4(\frac{\omega}{\kappa})^2] \tag{40}$$

When $\omega \ll \kappa$, this noise is a white noise and can be reduced with large optical power. However, increasing power will strengthen the backaction effect as discussed below.

5.3 Quantum backaction noise

The fluctuation of photon number will also disturb the optical force $F_{\rm opt}$ [See Eq. (13)]

$$S_{\rm FF}^{ba}(\omega) = \bar{n}_{\rm c}\frac{4\hbar^2 g_{\rm om}^2}{\kappa}\frac{1}{1 + (2\omega/\kappa)^2} \tag{41}$$

This force will introduce a quantum backaction displacement noise

$$S_{\rm xx}^{ba}(\omega) = |\chi_{\rm xx}|^2 S_{\rm FF}^{ba} \tag{42}$$

For a proper $\bar{n}_{\rm c}$, the sum of shot noise and backaction noise achieves a minimum value, which is the so-called standard quantum limit (SQL) [11]. If measured at the mechanical resonance, $\omega = \omega_{\rm m}$, it equals to $\hbar/(m_{\rm eff}\gamma_{\rm m}\omega_{\rm m})$, which correspond to zero-point fluctuations of the mechanical resonator with a measurement time $1/\gamma_{\rm m}$. This determines the ultra resolution which is independent of temperature.

5.4 Sensing towards quantum limit

From the discussion above, we find that thermal noise is an intrinsic property of a mechanical oscillator in contact with a heat bath at temperature T, while the contributions of shot noise and backaction noise are dependent on cavity photon number and optomechanical transduction mechanism. This provides us with flexible ways to control sensing performance. For thermal noise, one obvious optimization is to prepare mechanical resonators in the ground state, i.e., to lower its temperature. This should occur when $k_{\rm B}T/(\hbar\omega_{\rm m}) < 1$ and this cooling can also be achieved with optomechanical interaction [10]. For shot noise and backaction noise, they can be reconfigured with varying input power and also, tuned by optical spring and damping effect.

It should be noted that in different sensing application, these three types of noise may impose quite different requests on device design. For example, to decrease the noise level in displacement and mass sensing, high mechanical resonance frequency and small mass is generally preferred; for acceleration sensing, however, it is just the reverse since resonators with low mechanical frequency and large mass can induce a larger displacement shift when undergoing the same acceleration [see Eq. (24)].

6 Discussion and summary

Although the field of cavity optomechanics is still in its infancy, it is expanding rapidly both in terms of basic physics and applications [120–123]. More researchers are pulled into the field and more advanced devices are being developed. For sensing applications, cavity optomechanics possess certain advantages and challenges. For example, today most NEMS devices still require electrical actuation, which in many cases limits the operational bandwidth. Cavity optomechanical devices allow both optical actuation and readout, therefore providing faster sampling and scanning rates than electrical counterparts. Furthermore, G-Hz optomechanical devices at high frequencies directly links the signal domains at microwave frequencies in optical circuits, hence avoiding the complexity and cost of optoelectronic signal conversion [124]. On chip devices mentioned in this review all allow for the

integration of microlaser sources to replace the expensive and bulky external cavity lasers. In addition, optomechanical cavities can offer the unique resource of strong optical backaction effect. The optical spring and optical damping effect allows for dynamic tuning of the mechanical resonance frequency and bandwidth. Moreover, backaction cooling provides a scheme to damp or cool the mechanical resonator without degrading the resolution [79].

It is worth noting most experimental realizations till now has selected the material of devices as silicon, silicon nitride or silica, i.e., materials with large Young's modulus. One reason for this is the fabrication of these devices is compatible with CMOS technology; another is they generally have robust mechanical or optical properties such as high Q. However, the displacement of them driven by optical force is at most on the order of tens of nm, even in cavity enhanced systems designed to have reduced mechanical stiffness. To achieve larger sensitivity and tunability, it is meaningful to exploit mechanically compliant materials such as polymers, which can reduce cost and easily combine with microfluidic platforms.

In summary, we have described the basic physics, experimental systems and sensing applications in the context of cavity optomechanics. With currently rapid experimental success worldwide, it reveals an increasing chance to promote optomechanics from basic science to novel technologies. More and more optomechanical sensors are realized and their performance can already compete with their electronic counterparts. Looking into the future, the visionary role of cavity optomechanical sensing can be regarded as a light-mechanics interface to realize composite configurations integrating motion, mass or force sensors with information processing units within a monolithic photonic circuit.

Acknowledgements This work was supported by the National Basic Program of China (973 Program) (Grant No. 2013CB328704), the National Natural Science Foundation of China (Grants Nos. 11222440, 11004003, 11023003, and 1121091), the RFDPH (Grant No. 20120001110068), and Beijing Natural Science Foundation Program (Grant No. 4132058).

References and notes

1. J. Kepler, De Cometis, 1619
2. Actually Kepler's conjecture is not fully accurate. From the viewpoint of modern astronomy, the formation and deflection of comet tails are due to the forces from both radiation pressure and solar wind.
3. A. Ashkin, History of optical trapping and manipulation of small-neutral particle, atoms, and molecules, *IEEE J. Sel. Top. Quantum Electron.*, 2000, 6(6): 841
4. V. B. Braginsky and A. B. Manukin, Measurement of weak forces in physics experiments, Chicago: University of Chicago Press, 1977
5. K. J. Vahala, Optical microcavities, *Nature*, 2003, 424(6950): 839
6. J. Ma and M. L. Povinelli, Applications of optomechanical effects for on-chip manipulation of light signals, *Curr. Opin. Solid State Mater. Sci.*, 2012, 16(2): 82
7. H. Cai, K. Xu, A. Liu, Q. Fang, M. Yu, G. Lo, and D. Kwong, Nano-opto-mechanical actuator driven by gradient optical force, *Appl. Phys. Lett.*, 2012, 100(1): 013108
8. X. Guo, C. L. Zou, X. F. Ren, F. W. Sun, and G. C. Guo, Broadband opto-mechanical phase shifter for photonic integrated circuits, *Appl. Phys. Lett.*, 2012, 101(7): 071114
9. T. J. Kippenberg and K. J. Vahala, Cavity opto-mechanics, *Opt. Express*, 2007, 15(25): 17172
10. T. J. Kippenberg and K. J. Vahala, Cavity optomechanics: Back-action at the mesoscale, *Science*, 2008, 321(5893): 1172
11. A. A. Clerk, M. H. Devoret, S. M. Girvin, F. Marquardt, and R. J. Schoelkopf, Introduction to quantum noise, measurement, and amplification, *Rev. Mod. Phys.*, 2010, 82(2): 1155
12. P. Meystre, A short walk through quantum optomechanics, *Annalen der Physik*, 2013, 525(3): 215
13. M. Aspelmeyer, T. J. Kippenberg, and F. Marquardt, Cavity optomechanics, arXiv: 1303.0733, 2013
14. D. Van Thourhout and J. Roels, Optomechanical device actuation through the optical gradient force, *Nat. Photonics*, 2010, 4(4): 211
15. L. Atzori, A. Iera, and G. Morabito, The internet of things: A survey, *Comput. Netw.*, 2010, 54(15): 2787
16. A. B. Matsko, Practical Applications of Microresonators in Optics and Photonics, CRC Press, 2009
17. D. K. Armani, T. J. Kippenberg, S. M. Spillane, and K. J. Vahala, Ultra-high-Q toroid microcavity on a chip, *Nature*, 2003, 421(6926): 925
18. B. B. Li, Y. F. Xiao, C. L. Zou, X. F. Jiang, Y. C. Liu, F. W. Sun, Y. Li, and Q. Gong, Experimental controlling of Fano resonance in indirectly coupled whispering-gallery microresonators, *Appl. Phys. Lett.*, 2012, 100(2): 021108
19. Z. P. Liu, X. F. Jiang, Y. Li, Y. F. Xiao, L. Wang, J. L. Ren, S. J. Zhang, H. Yang, and Q. Gong, High-Q asymmetric polymer microcavities directly fabricated by two-photon polymerization, *Appl. Phys. Lett.*, 2013, 102(22): 221108
20. Y.-F. Xiao, X.-F. Jiang, Q.-F. Yang, L. Wang, K. Shi, Y. Li, and Q. Gong, Tunneling-induced transparency in a chaotic microcavity, *Laser & Photonics Reviews*, 2013, 7(5): L51
21. S. L. McCall, A. F. J. Levi, R. E. Slusher, S. J. Pearton, and R. A. Logan, Whispering-gallery mode microdisk lasers, *Appl. Phys. Lett.*, 1992, 60: 289
22. H. J. Moon, Y. T. Chough, and K. An, Cylindrical microcavity laser based on the evanescent-wave-coupled gain, *Phys. Rev. Lett.*, 2000, 85(15): 3161

23. X. F. Jiang, Y. F. Xiao, C. L. Zou, L. He, C. H. Dong, B. B. Li, Y. Li, F. W. Sun, L. Yang, and Q. Gong, Highly unidirectional emission and ultralow-threshold lasing from on-chip ultrahigh-Q microcavities, *Adv. Mater.*, 2012, 24(35): OP260
24. L. He, S. K. Özdemir, and L. Yang, Whispering gallery microcavity lasers, *Laser & Photonics Reviews*, 2013, 7: 60
25. B. B. Li, Y. F. Xiao, M. Y. Yan, W. R. Clements, and Q. Gong, Low-threshold Raman laser from an on-chip, high-Q, polymer-coated microcavity, *Opt. Lett.*, 2013, 38(11): 1802
26. Q. Xu, B. Schmidt, S. Pradhan, and M. Lipson, Micrometre-scale silicon electro-optic modulator, *Nature*, 2005, 435(7040): 325
27. H. Rokhsari and K. J. Vahala, Ultralow loss, high Q, four port resonant couplers for quantum optics and photonics, *Phys. Rev. Lett.*, 2004, 92(25): 253905
28. H. Lee, T. Chen, J. Li, O. Painter, and K. J. Vahala, Ultra-low-loss optical delay line on a silicon chip, *Nat. Commun.*, 2012, 3: 867
29. V. R. Almeida, C. A. Barrios, R. R. Panepucci, and M. Lipson, All-optical control of light on a silicon chip, *Nature*, 2004, 431(7012): 1081
30. J. Zhu, S. K. Ozdemir, Y. F. Xiao, L. Li, L. He, D. R. Chen, and L. Yang, On-chip single nanoparticle detection and sizing by mode splitting in an ultrahigh-Q microresonator, *Nat. Photonics*, 2009, 4(1): 46
31. F. Vollmer and S. Arnold, Whispering-gallery-mode biosensing: Label-free detection down to single molecules, *Nat. Methods*, 2008, 5(7): 591
32. X. Yi, Y. F. Xiao, Y. C. Liu, B. B. Li, Y. L. Chen, Y. Li, and Q. Gong, Multiple-Rayleigh-scatterer-induced mode splitting in a high-Q whispering-gallery-mode microresonator, *Phys. Rev. A*, 2011, 83(2): 023803
33. F. Vollmer and L. Yang, Review Label-free detection with high-Q microcavities: A review of biosensing mechanisms for integrated devices, *Nanophotonics*, 2012, 1(3–4): 267
34. L. Shao, X. F. Jiang, X. C. Yu, B. B. Li, W. R. Clements, F. Vollmer, W. Wang, Y. F. Xiao, and Q. Gong, Detection of single nanoparticles and lentiviruses using microcavity resonance broadening, *Adv. Mater.*, 2013, DOI: 10.1002/adma201302572
35. A. N. Cleland and M. L. Roukes, A nanometre-scale mechanical electrometer, *Nature*, 1998, 392: 160
36. K. Jensen, K. Kim, and A. Zettl, An atomic-resolution nanomechanical mass sensor, *Nat. Nanotechnol.*, 2008, 3(9): 533
37. J. L. Arlett, E. B. Myers, and M. L. Roukes, Comparative advantages of mechanical biosensors, *Nat. Nanotechnol.*, 2011, 6(4): 203
38. U. Krishnamoorthy, G. R. III Olsson, M. Bogart, D. Baker, T. Carr, T. P. Swiler, and P. Clews, In-plane MEMS-based nano-g accelerometer with sub-wavelength optical resonant sensor, *Sens. Actuators A Phys.*, 2008, 145: 283
39. M. O. Scully and M. S. Zubairy, Quantum Optics, Cambridge: Cambridge University Press, 1997
40. A. N. Cleland, Foundations of Nanomechanics: From Solid-State Theory to Device Applications, Springer-Verlag, 2003
41. C. Gardiner and P. Zoller, Quantum Noise, Springer, 2004
42. J. Rosenberg, Q. Lin, and O. Painter, Static and dynamic wavelength routing via the gradient optical force, *Nat. Photonics*, 2009, 3(8): 478
43. B. S. Sheard, M. B. Gray, C. M. Mow-Lowry, D. E. McClelland, and S. E. Whitcomb, Observation and characterization of an optical spring, *Phys. Rev. A*, 2004, 69(5): 051801
44. A. Baas, J. P. Karr, H. Eleuch, and E. Giacobino, Optical bistability in semiconductor microcavities, *Phys. Rev. A*, 2004, 69(2): 023809
45. Y. F. Yu, J. B. Zhang, T. Bourouina, and A. Q. Liu, Optical-force-induced bistability in nanomachined ring resonator systems, *Appl. Phys. Lett.*, 2012, 100(9): 093108
46. G. S. Wiederhecker, L. Chen, A. Gondarenko, and M. Lipson, Controlling photonic structures using optical forces, *Nature*, 2009, 462(7273): 633
47. A. Schliesser, P. Del'Haye, N. Nooshi, K. J. Vahala, and T. J. Kippenberg, Radiation pressure cooling of a micromechanical oscillator using dynamical backaction, *Phys. Rev. Lett.*, 2006, 97(24): 243905
48. O. Arcizet, P. F. Cohadon, T. Briant, M. Pinard, and A. Heidmann, Radiation-pressure cooling and optomechanical instability of a micromirror, *Nature*, 2006, 444(7115): 71
49. Y. C. Liu, Y. F. Xiao, X. Luan, and C. W. Wong, Dynamic dissipative cooling of a mechanical resonator in strong coupling optomechanics, *Phys. Rev. Lett.*, 2013, 110(15): 153606
50. T. Carmon, H. Rokhsari, L. Yang, T. J. Kippenberg, and K. J. Vahala, Temporal behavior of radiation-pressure-induced vibrations of an optical microcavity phonon mode, *Phys. Rev. Lett.*, 2005, 94(22): 223902
51. T. J. Kippenberg, H. Rokhsari, T. Carmon, A. Scherer, and K. J. Vahala, Analysis of radiation-pressure induced mechanical oscillation of an optical microcavity, *Phys. Rev. Lett.*, 2005, 95(3): 033901
52. K. Zandi, B. Wong, J. Zou, R. V. Kruzelecky, W. Jamroz, and Y. A. Peter, In-plane silicon-on-insulator optical MEMS accelerometer using waveguide fabry-perot microcavity with silicon/air bragg mirrors, in: IEEE 23rd International Conference on Micro Electro Mechanical Systems, IEEE, 2010: 839–842
53. M. W. Pruessner, T. H. Stievater, J. B. Khurgin, and W. S. Rabinovich, Integrated waveguide-DBR microcavity optomechanical system, *Opt. Express*, 2011, 19(22): 21904
54. B. E. Little, J. S. Foresi, G. Steinmeyer, E. R. Thoen, S. T. Chu, H. A. Haus, E. P. Ippen, L. C. Kimerling, and W. Greene, Ultra-compact Si-SiO_2 microring resonator optical channel dropping filters, *IEEE Photon. Technol. Lett.*, 1998, 10(4): 549

55. F. Xia, M. Rooks, L. Sekaric, and Y. Vlasov, Ultra-compact high order ring resonator filters using submicron silicon photonic wires for on-chip optical interconnects, *Opt. Express*, 2007, 15(19): 11934
56. W. H. P. Pernice, M. Li, and H. X. Tang, Optomechanical coupling in photonic crystal supported nanomechanical waveguides, *Opt. Express*, 2009, 17(15): 12424
57. M. Li, W. H. P. Pernice, and H. X. Tang, Ultrahigh-frequency nano-optomechanical resonators in slot waveguide ring cavities, *Appl. Phys. Lett.*, 2010, 97(18): 183110
58. A. N. Oraevsky, Whispering-gallery waves, *Quantum Electron.*, 2002, 32(5): 377
59. A. B. Matsko and V. S. Ilchenko, Optical resonators with whispering-gallery modes-part I: basics, *IEEE J. Sel. Top. Quantum Electron.*, 2006, 12(1): 3
60. G. Anetsberger, R. Rivi'ere, A. Schliesser, O. Arcizet, and T. J. Kippenberg, Ultralow-dissipation optomechanical resonators on a chip, *Nat. Photonics*, 2008, 2(10): 627
61. Q. Lin, J. Rosenberg, X. Jiang, K. J. Vahala, and O. Painter, Mechanical oscillation and cooling actuated by the optical gradient force, *Phys. Rev. Lett.*, 2009, 103(10): 103601
62. X. Jiang, Q. Lin, J. Rosenberg, K. Vahala, and O. Painter, High-Q double-disk microcavities for cavity optomechanics, *Opt. Express*, 2009, 17(23): 20911
63. Q. Lin, J. Rosenberg, D. Chang, R. Camacho, M. Eichenfield, K. J. Vahala, and O. Painter, Coherent mixing of mechanical excitations in nano-optomechanical structures, *Nat. Photonics*, 2010, 4(4): 236
64. S. Lee, S. C. Eom, J. S. Chang, C. Huh, G. Y. Sung, and J. H. Shin, A silicon nitride microdisk resonator with a 40-nm-thin horizontal air slot, *Opt. Express*, 2010, 18(11): 11209
65. S. Lee, S. C. Eom, J. S. Chang, C. Huh, G. Y. Sung, and J. H. Shin, Label-free optical biosensing using a horizontal air-slot SiN_x microdisk resonator, *Opt. Express*, 2010, 18(20): 20638
66. J. D. Thompson, B. M. Zwickl, A. M. Jayich, F. Marquardt, S. M. Girvin, and J. G. E. Harris, Strong dispersive coupling of a high-finesse cavity to a micromechanical membrane, *Nature*, 2008, 452(7183): 72
67. G. Anetsberger, O. Arcizet, Q. P. Unterreithmeier, R. Riviere, A. Schliesser, E. M. Weig, J. P. Kotthaus, and T. J. Kippenberg, Near-field cavity optomechanics with nanomechanical oscillators, *Nat. Phys.*, 2009, 5(12): 909
68. C. L. Zou, X. B. Zou, F. W. Sun, Z. F. Han, and G. C. Guo, Room-temperature steady-state optomechanical entanglement on a chip, *Phys. Rev. A*, 2011, 84(3): 032317
69. E. Gavartin, P. Verlot, and T. J. Kippenberg, A hybrid on-chip optomechanical transducer for ultrasensitive force measurements, *Nat. Nanotechnol.*, 2012, 7(8): 509
70. H. K. Li, Y. C. Liu, X. Yi, C. L. Zou, X. X. Ren, and Y. F. Xiao, Proposal for a near-field optomechanical system with enhanced linear and quadratic coupling, *Phys. Rev. A*, 2012, 85(5): 053832
71. J. Chan, M. Eichenfield, R. Camacho, and O. Painter, Optical and mechanical design of a "zipper" photonic crystal optomechanical cavity, *Opt. Express*, 2009, 17(5): 3802
72. M. Eichenfield, R. Camacho, J. Chan, K. J. Vahala, and O. Painter, A picogram- and nanometre-scale photonic-crystal optomechanical cavity, *Nature*, 2009, 459(7246): 550
73. M. Eichenfield, J. Chan, R. M. Camacho, K. J. Vahala, and O. Painter, Optomechanical crystals, *Nature*, 2009, 462(7269): 78
74. M. Notomi, H. Taniyama, S. Mitsugi, and E. Kuramochi, Optomechanical wavelength and energy conversion in high-Q double-layer cavities of photonic crystal slabs, *Phys. Rev. Lett.*, 2006, 97(2): 023903
75. X. Sun, J. Zheng, M. Poot, C. W. Wong, and H. X. Tang, Femtogram doubly clamped nanomechanical resonators embedded in a high-Q two-dimensional photonic crystal nanocavity, *Nano Lett.*, 2012, 12(5): 2299
76. G. Bahl, K. H. Kim,W. Lee, J. Liu, X. Fan, and T. Carmon, Brillouin cavity optomechanics with microfluidic devices, *Nat. Commun.*, 2013, 4: 1994
77. V. Ginis, P. Tassin, C. M. Soukoulis, and I. Veretennicoff, Enhancing optical gradient forces with metamaterials, *Phys. Rev. Lett.*, 2013, 110(5): 057401
78. K. Srinivasan, H. Miao, M. T. Rakher, M. Davanco, and V. Aksyuk, Optomechanical transduction of an integrated silicon cantilever probe using a microdisk resonator, *Nano Lett.*, 2011, 11(2): 791
79. A. G. Krause, M. Winger, T. D. Blasius, Q. Lin, and O. Painter, A high-resolution microchip optomechanical accelerometer, *Nat. Photonics*, 2012, 6(11): 768
80. M. L. Povinelli, S. G. Johnson, M. Loncar, M. Ibanescu, E. J. Smythe, F. Capasso, and J. D. Joannopoulos, High-Q enhancement of attractive and repulsive optical forces between coupled whispering-gallery-mode resonators, *Opt. Express*, 2005, 13(20): 8286
81. V. S. Ilchenko, M. L. Gorodetsky, and S. P. Vyatchanin, Coupling and tunability of optical whispering-gallery modes: A basis for coordinate meter, *Opt. Commun.*, 1994, 107(1–2): 41
82. J. L. Arlett, E. B. Myers, and M. L. Roukes, Comparative advantages of mechanical biosensors, *Nat. Nanotechnol.*, 2011, 6(4): 203
83. A. Boisen, S. Dohn, S. S. Keller, S. Schmid, and M. Tenje, Cantilever-like micromechanical sensors., *Rep. Prog. Phys.*, 2011, 74(3): 036101
84. Y. Liu, H. Miao, V. Aksyuk, and K. Srinivasan, Wide cantilever stiffness range cavity optomechanical sensors for atomic force microscopy, *Opt. Express*, 2012, 20(16): 18268
85. G. I. Harris, D. L. McAuslan, T. M. Stace, A. C. Doherty, and W. P. Bowen, Minimum requirements for feedback enhanced force sensing, arXiv: 1303.1589, 2013
86. D. Woolf, P. C. Hui, E. Iwase, M. Khan, A. W. Rodriguez, P. Deotare, I. Bulu, S. G. Johnson, F. Capasso, and M.

Loncar, Optomechanical and photothermal interactions in suspended photonic crystal membranes, *Opt. Express*, 2013, 21(6): 7258

87. F. Capasso, J. N. Munday, D. Iannuzzi, and H. B. Chan, Casimir forces and quantum electrodynamical torques: Physics and nanomechanics, *IEEE J. Sel. Top. Quantum Electron.*, 2007, 13(2): 400
88. A. W. Rodriguez, F. Capasso, and S. G. Johnson, The Casimir effect in microstructured geometries, *Nat. Photonics*, 2011, 5(4): 211
89. J. J. Li and K. D. Zhu, Nonlinear optical mass sensor with an optomechanical microresonator, *Appl. Phys. Lett.*, 2012, 101(14): 141905
90. F. Liu and M. Hossein-Zadeh, Mass sensing with optomechanical oscillation, *IEEE Sens. J.*, 2013, 13(1): 146
91. C. Gmachl, F. Capasso, E. Narimanov, J. U. N¨ockel, A. D. Stone, J. Faist, D. L. Sivco, and A. Y. Cho, High-power directional emission from microlasers with chaotic resonators, *Science*, 1998, 280(5369): 1556
92. Q. J. Wang, C. Yan, N. Yu, J. Unterhinninghofen, J. Wiersig, C. Pfl¨ugl, L. Diehl, T. Edamura, M. Yamanishi, H. Kan, and F. Capasso, From the cover: Whispering-gallery mode resonators for highly unidirectional laser action, *Proc. Natl. Acad. Sci. USA*, 2010, 107(52): 22407
93. C. L. Zou, F. J. Shu, F. W. Sun, Z. J. Gong, Z. F. Han, and G. C. Guo, Theory of free space coupling to high-Q whispering gallery modes, *Opt. Express*, 2013, 21(8): 9982
94. B. E. Little, S. T. Chu, H. A. Haus, J. Foresi, and J. P. Laine, Microring resonator channel dropping filters, *J. Lightwave Technol.*, 1997, 15(6): 998
95. J. P. Laine, B. E. Little, D. R. Lim, H. C. Tapalian, L. C. Kimerling, and H. A. Haus, Microsphere resonator mode characterization by pedestal anti-resonant reflecting waveguide coupler, *IEEE Photon. Technol. Lett.*, 2000, 12(8): 1004
96. J. P. Laine, C. Tapalian, B. Little, and H. Haus, Acceleration sensor based on high-Q optical microsphere resonator and pedestal antiresonant reflecting waveguide coupler, *Sens. Actuators A Phys.*, 2001, 93(1): 1
97. M. A. Perez and A. M. Shkel, Design and demonstration of a bulk micromachined Fabry–Pérot μg-resolution accelerometer, *IEEE Sens. J.*, 2007, 7(12): 1653
98. U. Krishnamoorthy, G. R. III Olsson, M. S. Bogart, D. W. Baker, T. P. Carr, T. P. Swiler, and P. J. Clews, In-plane MEMS-based nano-g accelerometer with sub-wavelength optical resonant sensor, *Sens. Actuators A Phys.*, 2008, 145–146: 283
99. D. N. Hutchison and S. A. Bhave, Z-axis optomechanical accelerometer, in: IEEE 25th International Conference on Micro Electro Mechanical Systems, IEEE, 2012: 615–619
100. P. H. Kim, C. Doolin, B. D. Hauer, A. J. MacDonald, M. R. Freeman, P. E. Barclay, and J. P. Davis, Nanoscale torsional optomechanics, *Appl. Phys. Lett.*, 2013, 102(5): 053102
101. J. P. Davis, D. Vick, D. C. Fortin, J. A. J. Burgess, W. K. Hiebert, and M. R. Freeman, Nanotorsional resonator torque magnetometry, *Appl. Phys. Lett.*, 2010, 96(7): 072513
102. S. Forstner, S. Prams, J. Knittel, E. D. van Ooijen, J. D. Swaim, G. I. Harris, A. Szorkovszky, W. P. Bowen, and H. Rubinsztein-Dunlop, Cavity optomechanical magnetometer, *Phys. Rev. Lett.*, 2012, 108(12): 120801
103. S. Lin, E. Schonbrun, and K. Crozier, Optical manipulation with planar silicon microring resonators, *Nano Lett.*, 2010, 10(7): 2408
104. H. Cai and A. W. Poon, Optical manipulation and transport of microparticles on silicon nitride microring-resonator-based add–drop devices, *Opt. Lett.*, 2010, 35(17): 2855
105. H. Cai and A. W. Poon, Optical manipulation of microparticles using whispering-gallery modes in a silicon nitride microdisk resonator, *Opt. Lett.*, 2011, 36(21): 4257
106. V. R. Dantham, S. Holler, V. Kolchenko, Z. Wan, and S. Arnold, Taking whispering gallery-mode single virus detection and sizing to the limit, *Appl. Phys. Lett.*, 2012, 101(4): 043704
107. S. I. Shopova, R. Rajmangal, S. Holler, and S. Arnold, Plasmonic enhancement of a whispering-gallery-mode biosensor for single nanoparticle detection, *Appl. Phys. Lett.*, 2011, 98(24): 243104
108. M. A. Santiago-Cordoba, M. Cetinkaya, S. V. Boriskina, F. Vollmer, and M. C. Demirel, Ultrasensitive detection of a protein by optical trapping in a photonic-plasmonic microcavity, *J. Biophoton.*, 2012, 5(8–9): 629
109. A. H. J. Yang, S. D. Moore, B. S. Schmidt, M. Klug, M. Lipson, and D. Erickson, Optical manipulation of nanoparticles and biomolecules in sub-wavelength slot waveguides, *Nature*, 2009, 457(7225): 71
110. S. Lin and K. B. Crozier, Planar silicon microrings as wavelength-multiplexed optical traps for storing and sensing particles, *Lab on a Chip*, 2011, 11(23): 4047
111. L. Novotny and B. Hecht, Principles of Nano-Optics, Cambridge: Cambridge University Press, 2006
112. J. D. Jackson, Classical Electrodynamics, Wiley, 1998
113. J. P. Gordon, Radiation forces and momenta in dielectric media, *Phys. Rev. A*, 1973, 8(1): 14
114. A. Ashkin, J. M. Dziedzic, J. E. Bjorkholm, and S. Chu, Observation of a single-beam gradient force optical trap for dielectric particles, *Opt. Lett.*, 1986, 11(5): 288
115. Y. F. Xiao, C. L. Zou, B. B. Li, Y. Li, C. H. Dong, Z. F. Han, and Q. Gong, High-Q exterior Whispering-Gallery modes in a metal-coated microresonator, *Phys. Rev. Lett.*, 2010, 105(15): 153902
116. Y. F. Xiao, Y. C. Liu, B. B. Li, Y. L. Chen, Y. Li, and Q. Gong, Strongly enhanced light-matter interaction in a hybrid photonic-plasmonic resonator, *Phys. Rev. A*, 2012, 85(3): 031805
117. L. Zhou, X. Sun, X. Li, and J. Chen, Miniature microring resonator sensor based on a hybrid plasmonic waveguide, *Sensors*, 2011, 11(12): 6856

118. Y. W. Hu, B. B. Li, Y. X. Liu, Y. F. Xiao, and Q. Gong, Hybrid photonic–plasmonic mode for refractometer and nanoparticle trapping, *Opt. Commun.*, 2013, 291: 380
119. F. Marquardt, J. P. Chen, A. A. Clerk, and S. M. Girvin, Quantum theory of cavity-assisted sideband cooling of mechanical motion, *Phys. Rev. Lett.*, 2007, 99(9): 093902
120. M. Ludwig and F. Marquardt, Quantum many-body dynamics in optomechanical arrays, *Phys. Rev. Lett.*, 2013, 111(7): 073603
121. M. A. Lemonde, N. Didier, and A. A. Clerk, Nonlinear interaction effects in a strongly driven optomechanical cavity, *Phys. Rev. Lett.*, 2013, 111(5): 053602
122. K. Børkje, A. Nunnenkamp, J. D. Teufel, and S. M. Girvin, Signatures of nonlinear cavity optomechanics in the weak coupling regime, *Phys. Rev. Lett.*, 2013, 111(5): 053603
123. Y. C. Liu, Y. F. Xiao, Y. L. Chen, X. C. Yu, and Q. Gong, Parametric down-conversion and polariton pair generation in optomechanical systems, *Phys. Rev. Lett.*, 2013, 111(8): 083601
124. J. Capmany and D. Novak, Microwave photonics combines two worlds, *Nat. Photonics*, 2007, 1(6): 319